Smart Structures and Systems, *Vol. 33, No. 2 (2024) 145-163*
https://doi.org/10.12989/sss.2024.33.2.145

Time-varying characteristics analysis of vehicle-bridge interaction system using an accurate time-frequency method

Tian-Li Huang [1a], Lei Tang [1b], Chen-Lu Zhan [1c], Xu-Qiang Shang [1d], Ning-Bo Wang*[1] and Wei-Xin Ren [2e]

[1] *School of Civil Engineering, Central South University, Changsha, Hunan 410075, China*
[2] *College of Civil and Transportation Engineering, Shenzhen University, Shenzhen, Guangdong 518061, China*

(*Received July 10, 2023, Revised January 9, 2024, Accepted January 10, 2024*)

Abstract. The evaluation of dynamic characteristics of bridges under operational traffic loads is a crucial aspect of bridge structural health monitoring. In the vehicle-bridge interaction (VBI) system, the vibration responses of bridge exhibit time-varying characteristics. To address this issue, an accurate time-frequency analysis method that combines the autoregressive power spectrum based empirical wavelet transform (AR-EWT) and local maximum synchrosqueezing transform (LMSST) is proposed to identify the time-varying instantaneous frequencies (IFs) of the bridge in the VBI system. The AR-EWT method decomposes the vibration response of the bridge into mono-component signals. Then, LMSST is employed to identify the IFs of each mono-component signal. The AR-EWT combined with the LMSST method (AR-EWT+LMSST) can resolve the problem that LMSST cannot effectively identify the multi-component signals with weak amplitude components. The proposed AR-EWT+LMSST method is compared with some advanced time-frequency analysis techniques such as synchrosqueezing transform (SST), synchroextracting transform (SET), and LMSST. The results demonstrate that the proposed AR-EWT+LMSST method can improve the accuracy of identified IFs. The effectiveness and applicability of the proposed method are validated through a multi-component signal, a VBI numerical model with a four-degree-of-freedom half-car, and a VBI model experiment. The effect of vehicle characteristics, vehicle speed, and road surface roughness on the identified IFs of bridge are investigated.

Keywords: autoregressive power spectrum based empirical wavelet transform (AR-EWT); local maximum synchrosqueezing transform (LMSST); time-varying characteristics; vehicle-bridge interaction (VBI) system

1. Introduction

Bridge structures are key components of transportation networks, and the structural health monitoring of bridges plays an important role for the safety and effective operation of bridges. As evaluation of the dynamic characteristics of bridges under operational traffic loads is a crucial aspect of bridge structural health monitoring, research on the vehicle-bridge interaction (VBI) system has attracted substantial interest (Jin *et al*. 2022, Stoura *et al*. 2021, Di Matteo *et al*. 2022, González *et al*. 2023). The VBI system is a dynamic system that is impacted by the presence of a vehicle acting as an additional mass on the bridge. As the vehicle travels on the bridge, the mass of the VBI system changes with the spatial position of the vehicle. Meanwhile, the damping of the vehicle affects the vibration of the VBI system (Bettinelli *et al*. 2022, Glatz and Fink 2021, Stoura and Dimitrakopoulos 2020). Under the coupling effect of vehicle and bridge, the dynamic property of the bridge is changed and the vibration responses of the bridge exhibit time-varying characteristics when vehicles cross the bridge (Li *et al*. 2022, Matsuoka *et al*. 2020, Stancioiu and Ouyang 2016). Kim *et al*. (2003) conducted an experiment to evaluate the impact of vehicle mass on the natural frequencies of a bridge subjected to traffic-induced excitation. A change of 5.4% in the natural frequencies of a short-span bridge was observed, which correlated with a 3.8% ratio between the mass of the vehicle and the bridge super-structure. Yang *et al*. (2013) constructed a theoretical framework of the frequency variation in the VBI system. To achieve better condition monitoring of bridges, it is essential to accurately describe the frequency variation in the VBI system.

The time-frequency analysis (TFA) approaches are powerful tools for representing time-varying instantaneous frequencies (IFs) of non-stationary signals. The Hilbert transform (HT), the short-time Fourier transform (STFT), and the wavelet transform (WT) are commonly used for identifying the IFs of time-varying structures (Feldman 2014, Nagarajaiah and Varadarajan 2005, Yang and Nagarajaiah 2014). Recently, these traditional TFA methods have been increasingly utilized for the parameter identification of VBI systems. Kong *et al*. (2016) extracted the bridge modal properties by the fast Fourier transformation (FFT) and STFT. Tan and Uddin (2020)

*Corresponding author, Ph.D., Associate Professor,
E-mail: wangnb@csu.edu.cn
[a] Ph.D., Professor, E-mail: htianli@csu.edu.cn
[b] Ph.D. Candidate, E-mail: lei_tang@csu.edu.cn
[c] Graduate Student, E-mail: 923240278@qq.com
[d] Ph.D. Candidate, E-mail: shangxq@csu.edu.cn
[e] Ph.D., Professor, E-mail: renwx@szu.edu.cn

ISSN: 1738-1584 (Print), 1738-1991 (Online)

presented a method based on HT and band-pass filter technique to detect the bridge frequency drop caused by the structural damage. Cantero *et al*. (2017) analyzed the changes of bridge frequencies and modes during the passage of a vehicle by using the continuous wavelet transform (CWT). However, conventional TFA methods cannot provide sufficient information on the dynamic characteristics of VBI systems due to their limited resolution. Therefore, it is necessary to develop effective methods for TF characteristic analysis of VBI system. To improve the accuracy of time-frequency representation, some advanced TFA methods have been developed. Daubechies *et al*. (2011) proposed the synchrosqueezed wavelet transform (WSST), which reassigns the TF coefficients of the wavelet transform along the frequency direction to obtain a high precise TF representation. Liu *et al*. (2015) utilized the WSST to identify the time-varying IFs of damaged structures. Mostafa *et al*. (2021) used the WSST to extract the IFs of a VBI system for the purpose of capturing the time-dependent resonances of the system. Based on the concept of synchrosqueezing, the STFT-based synchrosqueezed transform (FSST) was developed (Thakur and Wu 2011). However, the synchrosqueezing transform (SST) based methods yield heavily smeared TF representation when dealing with strong frequency-modulated (FM) signals or strong noisy signals. Therefore, some enhanced SST methods were proposed, such as the second-order SST (Oberlin *et al*. 2015), the synchroextracting transform (SET) (Yu *et al*. 2017), and the local maximum synchrosqueezing transform (LMSST) (Yu *et al*. 2019). Tan *et al*. (2023) investigated the time-varying frequencies of bridge in the VBI system using the second-order SST, and the comparison to WT and STFT showed that the second-order SST can significantly improve the energy concentration of the TF representation. Li *et al*. (2020) adopted the SET to extract the time-varying characteristics of bridge under the passage of vehicles. The recently proposed LMSST shows superior energy concentration compared to SST. Furthermore, LMSST has gained attention in various fields such as seismic data analysis (Mahdavi *et al*. 2021) and post-earthquake damage detection (Kumar *et al*. 2023).

It should be noted that the spectrums generated by TFA approaches can only obtain the energy distribution with time, and the extraction of each component still relies on the time-frequency ridge detection. Yu *et al*. (2019) implemented a ridge detection method in LMSST to extract the IFs. However, this ridge detection method cannot effectively decompose and extract the IF ridge for multi-component time-varying signals with weak amplitude components in LMSST. The adaptive signal decomposition method provides a potential solution to effectively address this problem and to better apply LMSST in identifying the time-varying characteristics of the bridge in the VBI system. By decomposing the non-stationary multi-component signals into mono-component signals, time-frequency analysis and ridge detection method can be applied individually to the mono-component signals. Empirical wavelet transform (EWT) is a new adaptive signal decomposition method proposed by Gilles (2013). Due to its computational efficiency and theoretical completeness, EWT has been successfully applied in mechanical fault diagnosis, seismic signal analysis and modal parameter identification of civil engineering structures (Merainani *et al*. 2017, Kalra *et al*. 2020, Wan *et al*. 2020). EWT constructs a wavelet filter bank by adaptively dividing the band boundary to extract the different components of the multi-component signal. EWT performs well in processing the non-stationary signals if the appropriate band boundary is obtained. Li *et al*. (2021) identified the time-varying parameter of bridges subject to moving vehicles based on EWT, and the results from numerical model and field experiment on the VBI system have shown that EWT can effectively identify the IFs of bridge.

This paper combines the autoregressive (AR) power spectrum based EWT (AR-EWT) method (Luo *et al*. 2018) with LMSST (AR-EWT+LMSST) to address the issue that LMSST cannot effectively identify the multi-component signals with weak amplitude components. The AR-EWT decomposes the multi-component signal into mono-component signals. Then, LMSST is used to perform time-frequency analysis on each mono-component signal, and the IFs of each mono-component is obtained using the ridge detection algorithm. The proposed AR-EWT+LMSST method can effectively identify the time-varying IFs of bridge in the VBI system.

The rest of this paper is organized as follows. Section 2 briefly introduces the basic theory of the proposed AR-EWT+LMSST method, and a multi-component time-varying signal is used to demonstrate the process of IF identification using the proposed method. Section 3 gives the formulation of the VBI numerical model using a four-degree-of-freedom half-car and the road surface roughness is included. Section 4 conducts a numerical simulation study on the VBI model to verify the feasibility of proposed method and to test the effect of different parameters on the frequency of the bridge. Experiment of a VBI model system is established in Section 5. Some conclusions are drawn in Section 6.

2. Theoretical background of proposed AR-EWT+LMSST technique

2.1 AR-EWT

The empirical wavelet transform (EWT) method extracts a series of compactly supported amplitude-modulated and frequency-modulated mono-components from a signal by adaptively designing a set of wavelet filters (Eq. (1)) based on the signal band boundary obtained from the Fourier spectrum. The detailed theoretical background can refer to Gilles (2013).

$$\phi_n(\omega) = \begin{cases} 1 & \text{if } |\omega| \le \omega_n - \tau_n \\ \cos\left[\frac{\pi}{2}\beta\left(\frac{1}{2\tau_n}\right)(|\omega| - \omega_n + \tau_n)\right] & \text{if } \omega_n - \tau_n \le |\omega| \le \omega_n + \tau_n \\ 0 & \text{otherwise} \end{cases} \tag{1}$$

$$\psi_n(\omega)=\begin{cases}1 & \text{if } \omega_n+\tau_n\le|\omega|\le\omega_{n+1}-\tau_{n+1}\\ \cos\left[\frac{\pi}{2}\beta\left(\frac{1}{2\tau_{n+1}}\right)(|\omega|-\omega_{n+1}+\tau_{n+1})\right] & \text{if } \omega_{n+1}-\tau_{n+1}\le|\omega|\le\omega_{n+1}+\tau_{n+1}\\ \sin\left[\frac{\pi}{2}\beta\left(\frac{1}{2\tau_n}\right)(|\omega|-\omega_n+\tau_n)\right] & \text{if } \omega_n-\tau_n\le|\omega|\le\omega_n+\tau_n\\ 0 & \text{otherwise}\end{cases} \tag{2}$$

where $\phi_n(\omega)$ and $\psi_n(\omega)$ are the empirical scaling function and the empirical wavelet function, respectively; ω_n denotes the boundaries between each segment ,where $\omega_0=0$ and $\omega_n=\pi$; $\tau_n=\gamma\times\omega_n$, where $0<\gamma<min_n\frac{\omega_{n+1}-\omega_n}{\omega_{n+1}+\omega_n}$; $\beta(x)$ is an auxiliary function, and it is expressed as

$$\phi_n(\omega)=\begin{cases}0 & \text{if } x\le 0\\ \beta(x)+\beta(1-x)=1 & \text{if } x\in[0,1]\\ 1 & \text{if } x\ge 1\end{cases} \tag{3}$$

Many polynomial functions satisfy these properties, a polynomial function defined as Eq. (4) is adopted in this study

$$\beta(x)=x^4(35-84x+70x^2-20x^3)\quad x\in[0,1] \tag{4}$$

The approximation coefficients $W_x(0,t)$ and detail coefficients $W_s(n,t)$ can be given as

$$\begin{aligned}W_s(0,t)=\langle s,\phi_1\rangle&=\int s(\tau)\overline{\phi_1(\tau-t)}dt\\&=F^{-1}\left(\hat{s}(\omega)\overline{\hat{\phi}_1(\omega)}\right)\end{aligned} \tag{5}$$

$$\begin{aligned}W_s(n,t)=\langle s,\psi_n\rangle&=\int s(\tau)\overline{\psi_n(\tau-t)}dt\\&=F^{-1}\left(\hat{s}(\omega)\overline{\hat{\psi}_n(\omega)}\right)\end{aligned} \tag{6}$$

where$\langle\cdot\rangle$is the inner product, $\overline{(\cdot)}$ is the complex conjugate, $\widehat{(\cdot)}$ is the Fourier transform, $F^{-1}(\cdot)$is the inverse Fourier transform.

The signal $s(t)$ can be decomposed into several mono-component modes as

$$\begin{aligned}s(t)&=s_0(t)+\sum_{n=1}^{N}s_n(t)\\&=W_s(0,t)*\phi_1(t)+\sum_{n=1}^{N}W_s(n,t)*\psi_n(t)\end{aligned} \tag{7}$$

where "$*$" is the convolution.

However, it is challenging to effectively determine the band boundary of the non-stationary signal based on the Fourier spectrum, particularly when significant noise exists. Compared with the Fourier spectrum, the AR power spectrum is smoother and has higher resolution (Luo *et al.* 2018). Therefore, the AR power spectrum is used to define the boundaries instead of the Fourier spectrum.

Assuming that a linear system is excited by white Gaussian noise $w(n)$ with mean of zero and variance of σ^2, the output of the linear system $f(n)$ is modeled using the AR model, as shown in the following expression

$$f(n)=-\sum_{k=1}^{p}a_kf(n-k)+w(n) \tag{8}$$

where $f(n)$ is the output of a linear system; p is the order of the AR model; a_k is the prediction coefficient of the AR model. The canonical expression of the AR model used to calculate a_k and σ^2 is written as

$$r_f(m)=\begin{cases}-\sum_{k=1}^{p}a_kr_f(k)+\sigma^2, & m=0\\ -\sum_{k=1}^{p}a_kr_f(m-k), & m\ge 1\end{cases} \tag{9}$$

The power spectrum of the AR model is defined as

$$P_{AR}=\frac{\sigma^2}{\left|1+\sum_{k=1}^{p}a_ke^{-i\omega k}\right|^2} \tag{10}$$

where i is the imaginary unit.

2.2 LMSST

A multi-component signal $s(t)\in L^2(\mathbb{R})$ with frequency-modulated (FM) and amplitude-modulated (AM) is considered as

$$s(t)=\sum_{k=1}^{K}s_k(t)=\sum_{k=1}^{K}A_k(t)e^{i\varphi_k(t)} \tag{11}$$

where $k\in\{1,\dots,K\}$, A_k and $\varphi_k(t)$ are the instantaneous amplitude (IA) and instantaneous phase (IP) of $s_k(t)$, respectively. The instantaneous frequency (IF) is defined as $\varphi_k'(t)$, and "$'$" denotes the derivative.

The STFT of $s(t)$ with respect to the real and even window $g(u)\in L^2(\mathbb{R})$ is expressed as

$$G(t,\omega)=\int_{-\infty}^{+\infty}g(u-t)s(u)e^{-i\omega(u-t)}du \tag{12}$$

Assuming that $\exists\varepsilon$ is sufficiently small, $|A_k'(t)|\le\varepsilon$ and $\left|\varphi_k''(t)\right|\le\varepsilon$ for $\forall t$. The $A_k(u)$ and $\varphi_k(u)$ at the time point t is expanded as $A_k(u)=A_k(t)$ and $\varphi_k'(u)=\varphi_k(t)+\varphi_k'(t)(u-t)$ according to the Taylor expansion, where the higher order terms are neglected. Therefore, the signal $s(u)$ is approximated by

$$s(u)=\sum_{k=1}^{K}A_k(t)e^{i\left(\varphi_k(t)+\varphi_k'(t)(u-t)\right)} \tag{13}$$

Substituting Eqs. (13) into (12), the STFT $G(t,\omega)$ of the signal $s(u)$ is obtained as

$$G(t,\omega)=\sum_{k=1}^{K}A_k(t)e^{i\varphi_k(t)}\hat{g}\left(\omega-\varphi_k'(t)\right) \tag{14}$$

where $\hat{g}(\cdot)$ is the Fourier transform of the window function, and it compactly supports in $[-\Delta_\omega,\Delta_\omega]$. Due to $\left|e^{i\varphi_k(t)}\right|=1$, the STFT amplitude $|G(t,\omega)|$ is expressed as

$$|G(t,\omega)|=\sum_{k=1}^{K}A_k(t)\hat{g}\left(\omega-\varphi_k'(t)\right) \tag{15}$$

According to Eq. (15), $|G(t,\omega)|$ reaches the maximum when $\hat{g}\left(\omega-\varphi_k'(t)\right)=\hat{g}(0)$, which means the energy of the TF representation concentrates on the IFs with a smeared energy distribution in the region $[\varphi_k'(t)-\Delta_\omega,\varphi_k'(t)+\Delta_\omega]$. To concentrate the blurry energy of the STFT spectrum, a frequency-reassignment operator $\omega_m(t,\omega)$ is defined

$$\omega_m(t,\omega)=\begin{cases}\underset{\omega}{argmax}|G(t,\omega)|, & \text{if } |G(t,\omega)|\neq 0\\ 0, & \text{if } |G(t,\omega)|=0\end{cases} \tag{16}$$

Assuming that two different modes are well separated by sufficient frequency distance, i.e.,$\varphi_{k+1}'(t)-\varphi_k'(t)>2\Delta_\omega$. Considering that the Fourier transform of the window function satisfies $\hat{g}(\omega)\leq\hat{g}(0)$, and then Eq. (16) is expressed as

$$\omega_m(t,\omega)=\begin{cases}\varphi_k'(t), & \text{if } \omega\in[\varphi_k'(t)-\Delta_\omega,\varphi_k'(t)+\Delta_\omega]\\ 0, & \text{otherwise}\end{cases} \tag{17}$$

LMSST expression is written as

$$LMSST(t,\eta)=\int_{-\infty}^{+\infty}G(t,\omega)\delta\left(\eta-\omega_m(t,\omega)\right)d\omega \tag{18}$$

where $\delta(\cdot)$ is the Dirac delta function.

A ridge detection algorithm is combined with the synchroextracting operator to extract the IF of each mono-component signal from TF representation. More details about its theoretical background can refer to Yu *et al.* (2019). The synchroextracting operator (SEO) is written as

$$SEO(t,\omega)=\begin{cases}1, & |\omega-\omega_m(t,\omega)|<\varepsilon\\ 0 & \text{otherwise}\end{cases} \tag{19}$$

The ridge detection algorithm is defined as

$$\begin{aligned}E\left(IF_k(t)\right)=&\int_{-\infty}^{+\infty}\left|\mathrm{TFR}\left(t,IF_k(t)\right)\right|^2dt\\&-\int_{-\infty}^{+\infty}\left(\lambda\cdot IF_k'(t)^2+\beta\cdot IF_k''(t)^2\right)dt\end{aligned} \tag{20}$$

where the $\left(t,IF_k(t)\right)$ is the estimated IF of the k -th mode, and the SEO is used to estimate the IF; λ and β are used to adjust the regularization level.

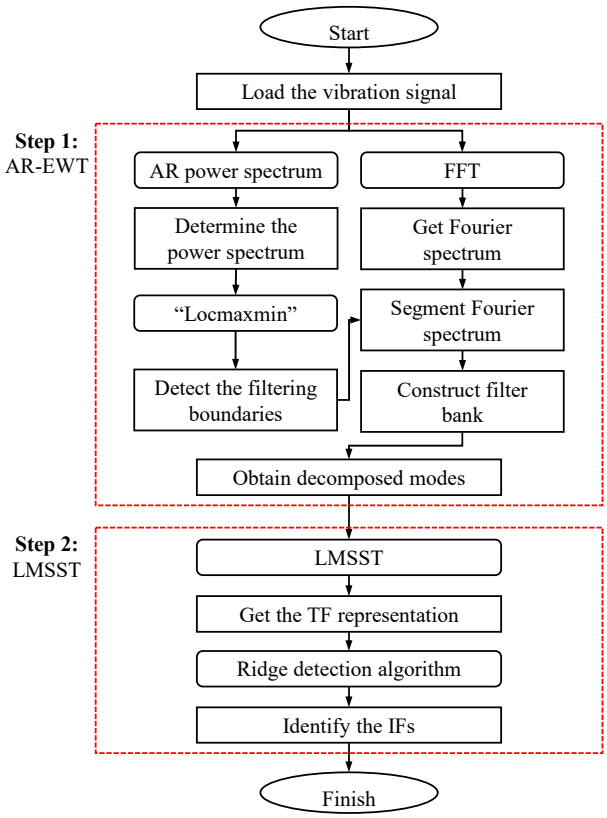

Fig. 1 Flowchart of the proposed AR-EWT+LMSST method for IF identification

2.3 Proposed AR-EWT+LMSST for IF identification

A method combining the AR-EWT and LMSST (AR-EWT+LMSST) is proposed to address the problem that LMSST cannot effectively identify the IFs of multi-component time-varying signals with weak amplitude components. The multi-component signal can be decomposed into different mono-component signals using AR-EWT. Then, LMSST (Eq. (18)) is used to perform time-frequency analysis on each mono-component signal, and the IFs of each mono-component is obtained using the ridge detection algorithm (Eqs. (19) and (20)). In AR-EWT, the "Locmaxmin" boundary detection method (Gilles 2013) is adopted to determine the boundaries in AR power spectrum (Eq. (10)) based on the minimum value between adjacent maximum points, and then the Fourier spectrum is segmented using the estimated boundaries to construct the filter bank (Eqs. (1) and (2)). The flowchart of the proposed method for IF identification is shown in Fig. 1.

2.4 Demonstration

A synthetic multi-component time-varying signal $S(t)$ is used to demonstrate the process of proposed AR-EWT+LMSST method for IF identification. The signal $S(t)$ consists of two component signals $s_1(t)$ and $s_2(t)$, and the corresponding theoretical IF of each component signal are $f_1=6+\cos(2.5t)$ Hz and $f_2=10+1.3\cos(0.65t)$ Hz, respectively. The sampling frequency is

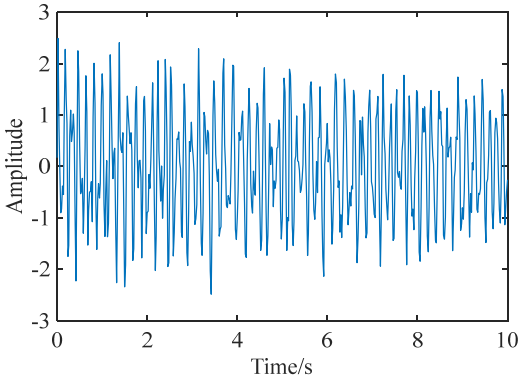

Fig. 2 Synthetic signal $S(t)$ with noise

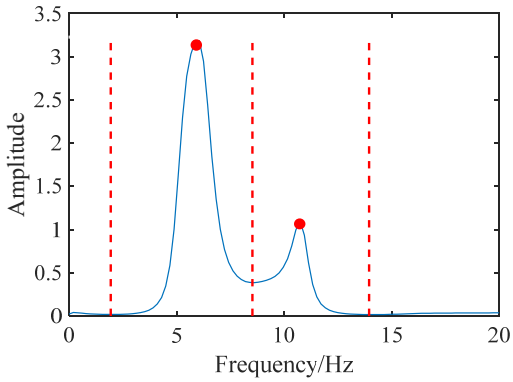

Fig. 3 AR power spectrum of signal $S(t)$

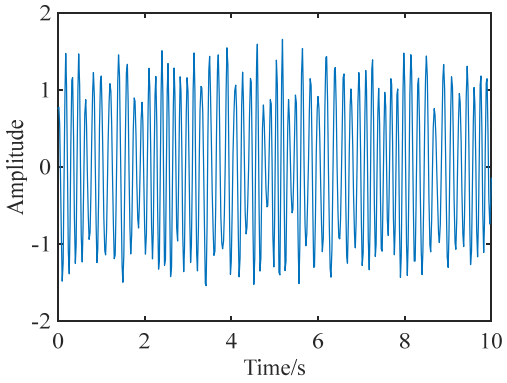

(a) First mode

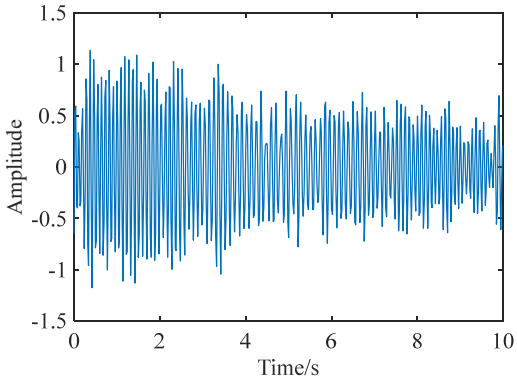

(b) Second mode

Fig. 4 The decomposed components of signal $S(t)$ using AR-EWT

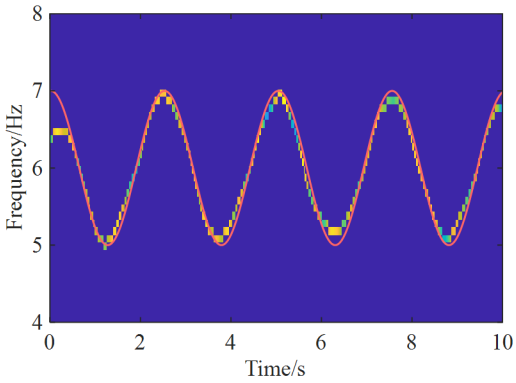

(a) First mode

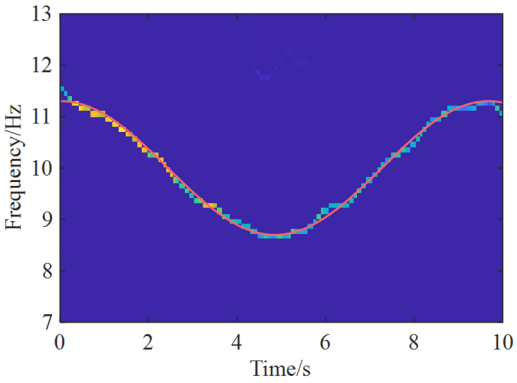

(b) Second mode

Fig. 5 LMSST spectrum for two modes

50 Hz and the time length is 10 s. The white Gaussian noise with signal to noise ratio (SNR) of 10 dB is added to the signal $S(t)$. Figs. 2 and 3 shows the synthetic signal with noise and the AR power spectrum, respectively. According to the AR power spectrum, two frequency components are clearly separated. Fig. 4 shows the two decomposed modes of signal $S(t)$ using AR-EWT. The TF representation of decomposed two modes obtained using LMSST are shown in Fig. 5. It can be seen that the energy of the LMSST spectrum for both the first mode and the second mode is highly concentrated and very consistent with the theoretical value (red solid line) in Fig. 5.

A comparison between the proposed AR-EWT+LMSST method and the LMSST, SST, and SET methods is conducted to demonstrate its effectiveness and accuracy. Fig. 6 shows the TF representation of signal $S(t)$ obtained by using SST, SET, and LMSST, as well as the theoretical IFs. Fig. 6(b) indicates that the IFs of the first mode in the LMSST spectrum is clear, but the energy of the second mode is barely detectable. This is because that the energy of the second mode is much lower than the first mode and low energy component is easily disturbed by noise. From Figs.

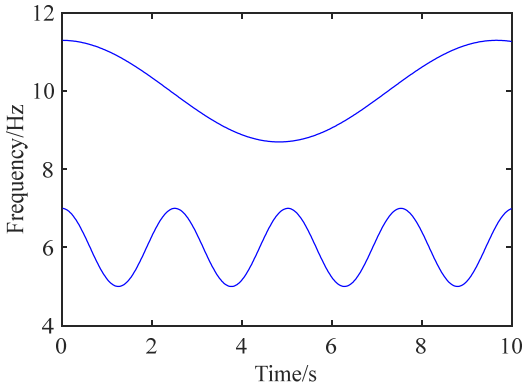

(a) Theoretical IFs

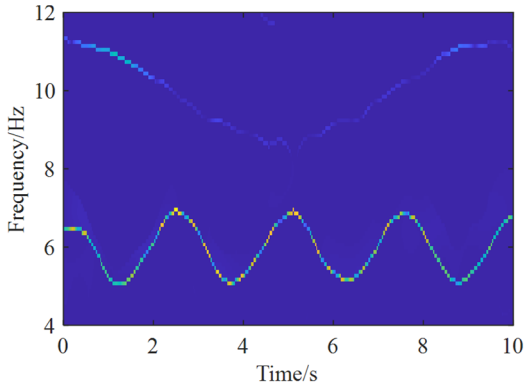

(a) Theoretical IFs

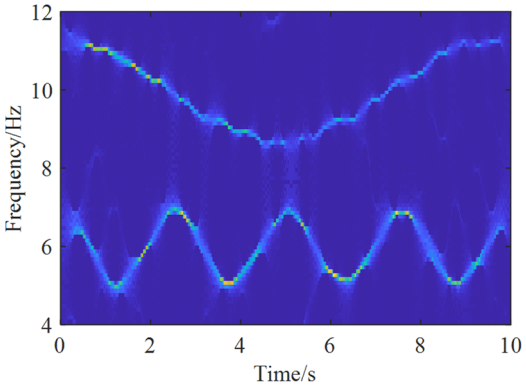

(c) SST spectrum

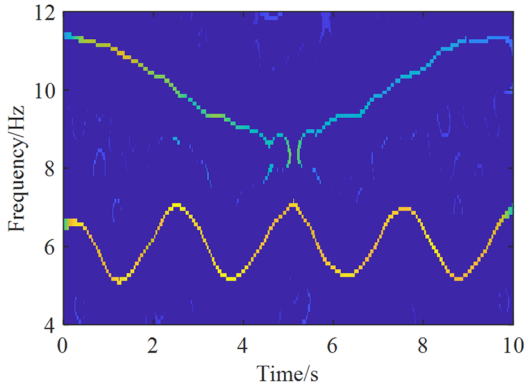

(d) SET spectrum

Fig. 6 Theoretical IFs and time-frequency spectrum

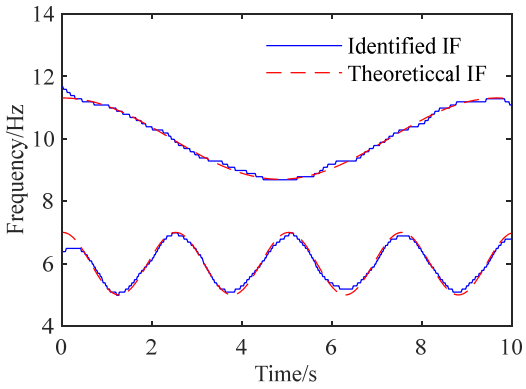

(a) Proposed AR-EWT+LMSST

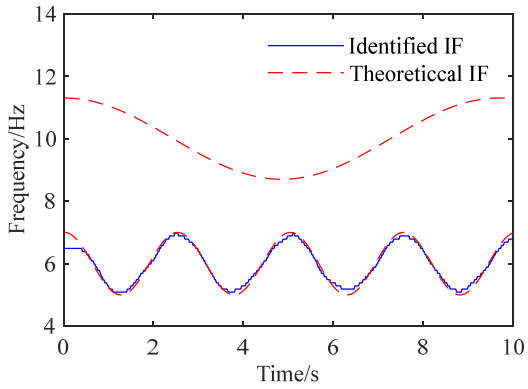

(b) LMSST

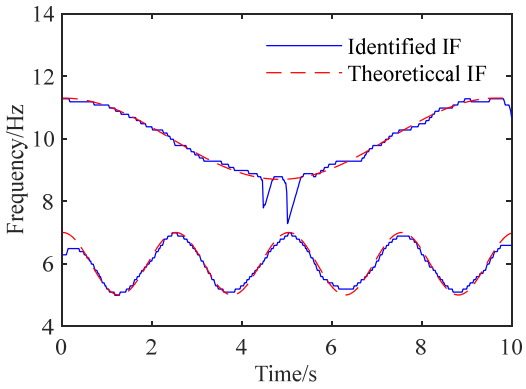

(c) SST

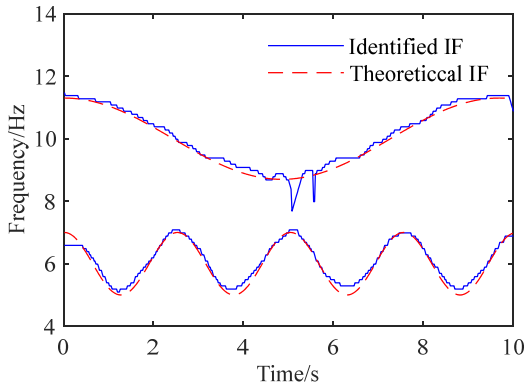

(d) SET

Fig. 7 Identified IFs of signal $S(t)$ using proposed AR-EWT+LMSST, LMSST, SST, and SET

Table 1 RMSE and MAE values of identified IFs of signal $S(t)$ by using four different TFA methods

Mode	Index	TFA method			
		AR-EWT+LMSST	LMSST	SST	SET
1	RMSE	0.1282	0.1290	0.1457	0.1518
	MAE	0.0982	0.1028	0.1064	0.1244
2	RMSE	0.0728	/	0.1955	0.1664
	MAE	0.0540	/	0.0975	0.1218

6(c) and 6(d), it can be seen that the IFs obtained by using SST and SET are blurry or even locally missing. The TF representation obtained by using the proposed AR-EWT+LMSST method (Fig. 5) is superior to the TF representations obtained by using the LMSST, SST, and SET methods.

The ridge detection algorithm is used to extract the IFs from the TF representation generated by using the AR-EWT+LMSST, LMSST, SST, and SET methods, as shown in Fig. 7, and the theoretical IFs is also presented in Fig. 7 for comparison. The IFs extracted from the TF representation generated by using the AR-EWT+LMSST method (Fig. 7(a)) is in good agreement with the theoretical IFs. However, due to the weak energy of the second mode, the IFs of the second mode cannot be identified by using LMSST method, as illustrated in Fig. 7(b). The SST (Fig. 7(c)) and SET (Fig. 7(d)) methods are able to identify the IFs of the two modes, but the extracted IFs show significant local fluctuations due to the blurry TF representation obtained from SST and SET.

To quantitatively evaluate the effectiveness and accuracy in identifying IF, the root mean square error (RMSE) and mean absolute error (MAE) are adopted

$$RMSE = \sqrt{\frac{1}{m}\sum_{i=1}^{m}(h(x_i) - y_i)^2} \tag{21}$$

$$MAE = \frac{1}{m}\sum_{i=1}^{m}|h(x_i) - y_i| \tag{22}$$

where m is number of sample points, $h(x_i)$ is the identified IFs, and y_i is the theoretical IFs.

Table 1 presents the RMSE and MAE values of identified IFs of signal $S(t)$ by using four different TFA methods. The identification accuracy of SST, SET, and LMSST is lower than that of AR-EWT+LMSST, as indicated by their higher RMSE and MAE values.

3. Theoretical background of VBI system

Fig. 8 illustrates a vehicle-bridge interaction (VBI) model, where the vehicle is modeled as a four-degree-of-freedom half-car model, and the bridge is modeled as a simply supported beam (Zhu and Law 2003). L, EI and ρ are the span, bending stiffness and linear density of the bridge, respectively. S is the vehicle length. a_1 and a_2 are the ratio of distance between the center of the vehicle and each axle to the wheelbase, respectively. I_v is the moment of inertia of the vehicle. m_v is the vehicle mass, m_1 and m_2 are the axle masss of axle 1 and 2, respectively. K_{s1} and K_{s2} are the vertical stiffness of the suspension of axle 1 and 2, respectively. K_{t1} and K_{t2} are the vertical stiffness of the tire of axle 1 and 2, respectively. C_{s1} and C_{s2} are the vertical dampers of the suspension of axle 1 and 2, respectively. C_{t1} and C_{t2} are the vertical dampers of the tire of axle 1 and 2, respectively.

Neglecting the coupling effect, the vehicle and bridge are two independent free vibration systems, and the equation of motion of vehicle and bridge are respectively expressed

$$M_v\ddot{y}_v + C_v\dot{y}_v + K_v y_v = 0 \tag{23}$$

$$M_b\ddot{y}_b + C_b\dot{y}_b + K_b y_b = 0 \tag{24}$$

where M_v, C_v and K_v represent the mass, damping, and stiffness matrices of the vehicle, respectively; M_b, C_b and K_b represent the mass, damping, and stiffness matrices of the bridge, respectively.

According to the principle of constant value of dynamic potential energy, the mass, stiffness and damping matrix in the equation of motion of vehicle (Eq. (23)) are written as follows

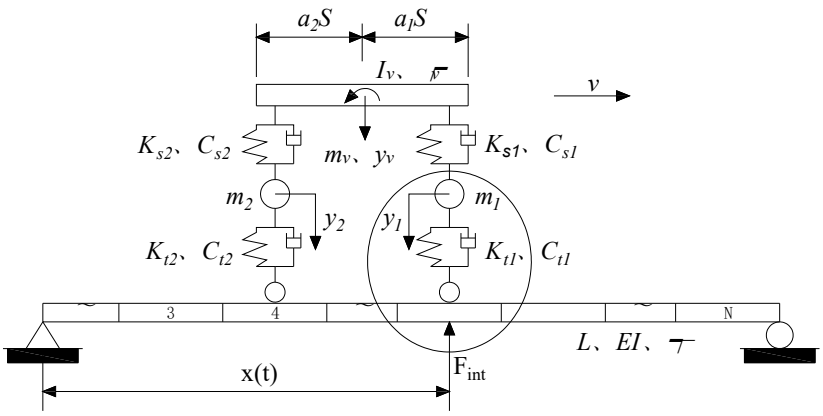

Fig. 8 Vehicle-bridge interaction model

$$M_v = diag[m_v \quad I_v \quad m_1 \quad m_2] \tag{25}$$

$$C_v = \begin{bmatrix} C_{s1}+C_{s2} & -l_1C_{s1}+l_2C_{s2} & -C_{s1} & -C_{s2} \\ -l_1C_{s1}+l_2C_{s2} & l_1^2C_{s1}+l_2^2C_{s2} & l_1C_{s1} & -l_2C_{s2} \\ -C_{s1} & l_1C_{s1} & C_{s1} & 0 \\ -C_{s2} & -l_2C_{s2} & 0 & C_{s2} \end{bmatrix} \tag{26}$$

$$K_v = \begin{bmatrix} K_{s1}+K_{s2} & -l_1K_{s1}+l_2K_{s2} & -K_{s1} & -K_{s2} \\ -l_1K_{s1}+l_2K_{s2} & l_1^2K_{s1}+l_2^2K_{s2} & l_1K_{s1} & -l_2K_{s2} \\ -K_{s1} & l_1K_{s1} & K_{s1} & 0 \\ -K_{s2} & -l_2K_{s2} & 0 & K_{s2} \end{bmatrix} \tag{27}$$

where $l_1 = a_1S$ and $l_2 = a_2S$.

Combing Eqs. (23) and (24), the time-invariant part of the equation of motion of VBI system is expressed as

$$\begin{bmatrix} M_v & \\ & M_b \end{bmatrix}\begin{Bmatrix} \ddot{y}_v \\ \ddot{y}_b \end{Bmatrix} + \begin{bmatrix} C_v & \\ & C_b \end{bmatrix}\begin{Bmatrix} \dot{y}_v \\ \dot{y}_b \end{Bmatrix} + \begin{bmatrix} K_v & \\ & K_b \end{bmatrix}\begin{Bmatrix} y_v \\ y_b \end{Bmatrix} = \begin{Bmatrix} 0 \\ 0 \end{Bmatrix} \tag{28}$$

Considering the coupling effect and the time-varying characteristics of the system caused by the vehicle driving on the bridge, as shown in the elliptical circle in Fig. 8. System coupling occurs due to the wheel's vertical motion and the deflection of the bridge deck's contact point. Since each node of the beam element only considers two degrees of freedom, i.e., rotation and deflection, each coupling involves a total of five degrees of freedom, including the six degrees of freedom of the two nodes of the beam element y_{bj} and the one vertical degree of freedom of the vehicle axle y_a. Taking the first wheel of the vehicle as an example, its coupling model can be expressed as

$$M_{int\_1}\begin{Bmatrix} \ddot{y}_{a1} \\ \ddot{y}_{bj1} \end{Bmatrix} + C_{int\_1}\begin{Bmatrix} \dot{y}_{a1} \\ \dot{y}_{bj1} \end{Bmatrix} + K_{int\_1}\begin{Bmatrix} y_{a1} \\ y_{bj1} \end{Bmatrix} = F_{int\_1} \tag{29}$$

$$M_{int\_1} = 0 \tag{30}$$

$$C_{int\_1} = \begin{bmatrix} C_{t1} & -C_{t1}N_{x=x_i} \\ -N^T{}_{x=x_i}C_{t1} & N^T{}_{x=x_i}C_{t1}N_{x=x_i} \end{bmatrix} \tag{31}$$

$$K_{int\_1} = \begin{bmatrix} K_{t1} & -K_{t1}N_{x=x_i} - C_{t1}vN'_{x=x_i} \\ -N^T{}_{x=x_i}K_{t1} & N^T{}_{x=x_i}K_{t1}N_{x=x_i} + N^T{}_{x=x_i}C_{t1}vN'_{x=x_i} \end{bmatrix} \tag{32}$$

$$F_{int\_1} = \begin{Bmatrix} K_{t1}r(x_i) + C_{t1}vr'(x_i) \\ \left(a_1m_v + m_1 - K_{t1}r(x_i) - C_{t1}vr'(x_i)\right)N_{x=x_i} \end{Bmatrix} \tag{33}$$

$$N = \begin{bmatrix} 1-10\left(\frac{x}{L}\right)^3+15\left(\frac{x}{L}\right)^4-6\left(\frac{x}{L}\right)^5 \\ x-6L\left(\frac{x}{L}\right)^3+8L\left(\frac{x}{L}\right)^4-3L\left(\frac{x}{L}\right)^5 \\ \frac{1}{2}x^2-\frac{3}{2}L^2\left(\frac{x}{L}\right)^3+\frac{3}{2}L^2\left(\frac{x}{L}\right)^4-\frac{1}{2}L^2\left(\frac{x}{L}\right)^5 \\ 10\left(\frac{x}{L}\right)^3-15\left(\frac{x}{L}\right)^4+6\left(\frac{x}{L}\right)^5 \\ -4L\left(\frac{x}{L}\right)^3+7L\left(\frac{x}{L}\right)^4-3L\left(\frac{x}{L}\right)^5 \\ \frac{1}{2}L^2\left(\frac{x}{L}\right)^3-L^2\left(\frac{x}{L}\right)^4+\frac{1}{2}L^2\left(\frac{x}{L}\right)^5 \end{bmatrix}^T \tag{34}$$

where N is the beam element shape function matrix, using Hermitian quintile spline function; x represents the distance between the coupling contact point and the left end of the beam; x_i is the value of x at a time; v represents the driving speed; $r(x)$ represents the road roughness, which is obtained by inverting the Fourier transform of the power spectral density function of the road, and its discrete form is expressed as

$$r(x) = \sum_{i=1}^{N}\sqrt{4G_d(n_i)\Delta n}\,cos(2\pi n_i + \theta_i) \tag{35}$$

where N is the number of sample point; $\Delta n = 1/N\Delta$, $n_i = i\cdot\Delta n$, Δ is the discrete distance interval; θ_i is the independent random phase angle uniformly distributed between $0 \sim 2\pi$; $G_d(n_i)$ is the power spectral density function of road.

For the vehicle-bridge interaction system, calculation of the road power spectral density should not only consider the road roughness but also the driving speed. This requires the transformation of spatial power spectrum into temporal power spectrum. The general expression for the temporal power spectrum is given as

$$G_d(f) = 4\pi^2G_d(n_0)n_0^2v \tag{36}$$

where $f = nv$ is the temporal frequency with a unit of Hz; n is the spatial frequency with a unit of cycle/m; $n_0 = 0.1$cycle/m is reference spatial frequency; $G_d(n_0)$ is the coefficient of road surface roughness with a unit of m^3/cycle.

Similarly, the coupling model of the second round pair and the bridge can be expressed as

$$M_{int\_2}\begin{Bmatrix} \ddot{y}_{a2} \\ \ddot{y}_{bj2} \end{Bmatrix} + C_{int\_2}\begin{Bmatrix} \dot{y}_{a2} \\ \dot{y}_{bj2} \end{Bmatrix} + K_{int\_2}\begin{Bmatrix} y_{a2} \\ y_{bj2} \end{Bmatrix} = F_{int\_2} \tag{37}$$

Table 2 Mechanical parameters of bridge in VBI system

Parameter	Value	Parameter	Value	Parameter	Value
L	32 m	EI	$9.4 \times 10^9 N \cdot m^2$	ρ	5×10^3kg/m

Table 3 Mechanical parameters of vehicle in VBI system

Parameter	Value	Parameter	Value	Parameter	Value
m_v	17000 kg	K_{s2}	2400 kN/m	C_{t1}	6 kN · s/m
I_v	40000 kg · m^2	K_{t1}	4800 kN/m	C_{t2}	12 kN · s/m
m_1	400 kg	K_{t2}	4800 kN/m	S	8 m
m_2	600 kg	C_{s1}	10 kN · s/m	a_1	0.5
K_{s1}	2400 kN/m	C_{s2}	20 kN · s/m	a_2	0.5

The stiffness, damping matrix and load array in Eqs. (29) and (37) are time-varying, which are represented as time-varying parts in the VBI system, corresponding to the degrees of freedom of the coupling part in the system.

When the vehicle crosses the bridge, the time-invariant part (Eq. (28)) the time-varying part (Eqs. (29) and (37)) are combined to obtain the equation of motion of VBI system.

4. Numerical simulation

4.1 Time-frequency analysis of bridge responses in VBI system

A numerical simulation of the VBI system is carried out using a simply supported beam bridge with a span of 32 meters and a four-degree-of-freedom half-car model. The vehicle-bridge model is shown in Fig. 8. The damping of the bridge is expressed by Rayleigh damping as $C_b = \xi_1 M_b + \xi_2 K_b$, and $\xi_1 = 0.4229$, $\xi_2 = 6.0536 \times 10^{-4}$. The mechanical parameters of bridge and vehicle in Fig. 8 are listed in Tables 2 and 3, respectively.

Considering the mechanical parameters of both the bridge and vehicle, a time-varying VBI model system is established based on MATLAB numerical computing platform and the bridge response of the VBI system can be calculated. The fundamental frequency of the vehicle is 2.17 Hz, while the first two frequencies of the bridge are 2.10 Hz and 8.41 Hz, respectively. The vehicle-bridge fundamental frequency ratio is 1.03, and the mass ratio is 0.11. With an assumption of a smooth road surface, the vibration equation of the VBI system is solved using the Wilson-θ integration method at a response frequency of 1000 Hz as the vehicle traveled at a speed of 7.2 km/h on the bridge. The vertical acceleration responses of the bridge is recorded from the front axle entering the bridge to the rear axle leaving the bridge. Fig. 9 shows the simulated vertical acceleration responses of the bridge at L/4 measurement point under a moving vehicle.

The proposed AR-EWT+LMSST method is employed to analyze the acceleration response of bridge. Fig. 10 shows the boundary bands divided in the AR power spectrum of the response signal, which clearly separate the first two order frequencies of the bridge. Therefore, AR-EWT can be

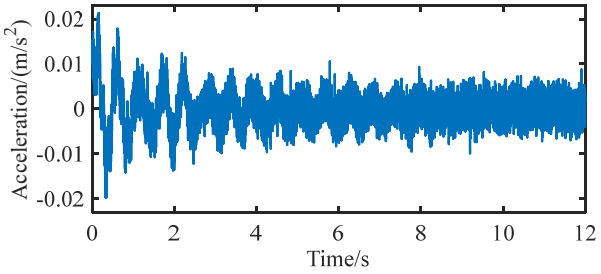

Fig. 9 Simulated vertical acceleration responses of the bridge at L/4 measurement point under a moving vehicle

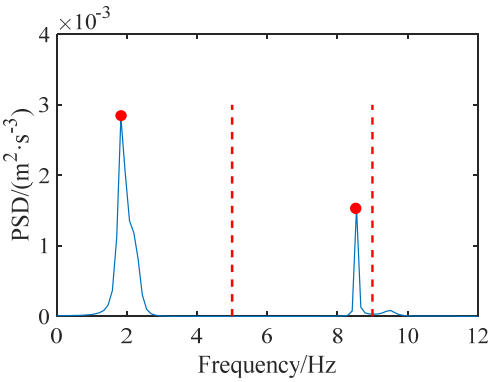

Fig. 10 AR power spectrum

used to effectively decompose the first two order frequencies of the bridge. LMSST is used to obtain the TF representation of the first and second frequency, as shown in Figs. 11(a) and 11(b). The IF detected by using ridge detection algorithm is displayed in Figs. 11(c) and 11(d). The identified IFs agree well with the theoretical IFs, indicating that the proposed AR-EWT+LMSST method can effectively identify the time-varying IFs of the bridge under a moving vehicle.

The SST, SET, and LMSST methods are used to analyze the acceleration response signal of the bridge, and the identified IFs are shown in Fig. 12. The first and second order frequencies obtained from SST and SET present abrupt change, especially the second order frequency, which

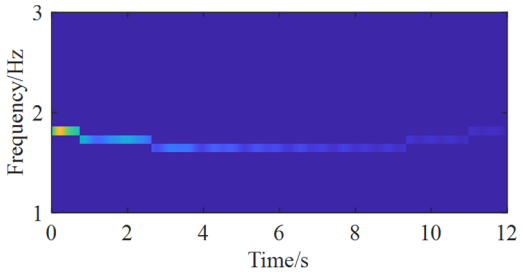

(a) LMSST spectrum of first order frequency

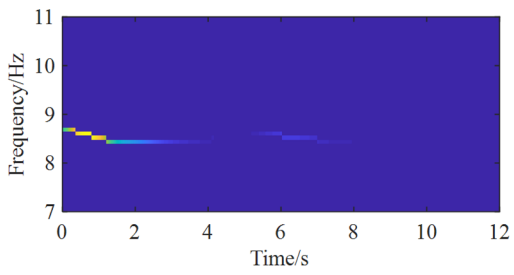

(b) LMSST spectrum of second order frequency

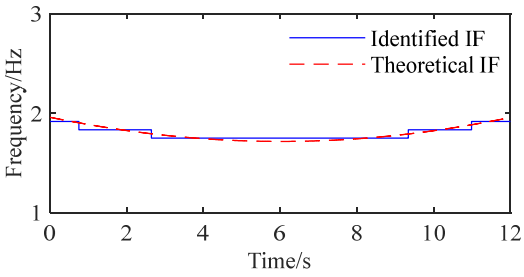

(c) First order frequency

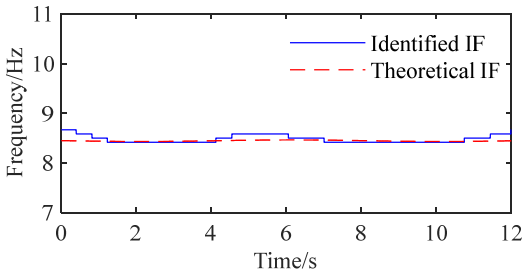

(d) Second order frequency

Fig. 11 LMSST spectrum and identified IFs using proposed AR-EWT+LMSST

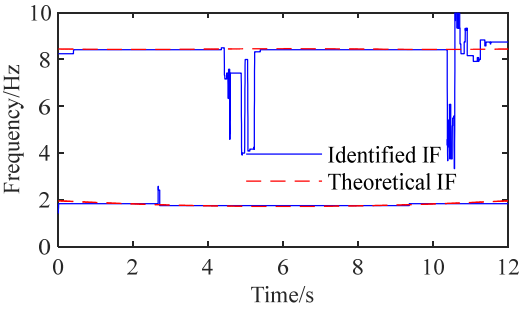

(a) SST

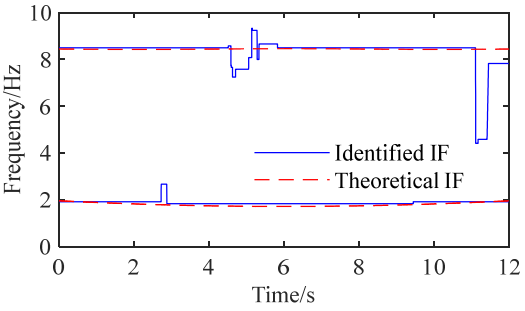

(b) SET

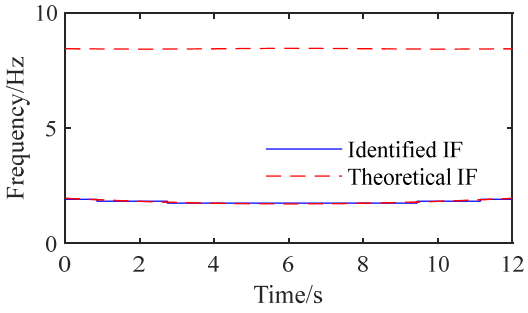

(c) LMSST

Fig. 12 Identified IFs by using SST, SET and LMSST

undergoes severe abrupt changes because the energy of the second order frequency is weak. LMSST accurately identifies the first order frequency but failed to identify the second order frequency. Table 4 presents the RMSE and MAE values of identified IFs of bridge in VBI system using four different TFA techniques, i.e., SST, SET, LMSST and AR-EWT+LMSST. The proposed AR-EWT+LMSST method exhibits the highest accuracy.

Table 4 RMSE and MAE values of identified IFs of bridge in VBI system using different TFA techniques

Frequency order	Index	TFA techniques			
		AR-EWT +LMSST	LMSST	SST	SET
1	RMSE	0.0259	0.0258	0.0579	0.1287
	MAE	0.0223	0.0222	0.0352	0.0862
2	RMSE	0.0775	/	0.9053	0.6845
	MAE	0.0575	/	0.3004	0.2396

4.2 Parametric analysis

The time-varying characteristics of the bridge under a moving vehicle are affected by various factors, such as vehicle properties (stiffness and mass), vehicle speed, and road surface roughness. This section aims to investigate the time-varying characteristics of VBI system under various factors using the proposed AR-EWT+LMSST method to identify the IF from the simulated acceleration responses of bridge.

4.2.1 Vehicle/bridge frequency ratio and vehicle/bridge mass ratio

Table 5 lists the mechanical properties of VBI system for four different vehicle models, including the vehicle stiffness, the vehicle mass, the vehicle/bridge frequency ratio and the vehicle/bridge mass ratio. To investigate the impact of the vehicle stiffness on the time-varying characteristics of the bridge, the vehicle mass is kept constant at m_v=18000 kg. The stiffness parameters of the vehicle shown in Table 3 are used as the standard parameter, and the overall vehicle stiffness is set as K_v. It can be observed from Table 5 that the vehicle/bridge frequency ratio decreases as the vehicle stiffness decreases.

The first two frequencies of bridge identified by AR-EWT+LMSST for different vehicle stiffness (Case1 to Case4) are shown in Fig. 13(a). As the vehicle moves on the bridge, the first order frequencies in four cases exhibit roughly half sine wave variations. The influence of the vehicle stiffness on the frequency of the VBI system is related to the vehicle/bridge frequency ratio. When vehicle/bridge frequency ratio is larger than 1, the first order frequency of the bridge decreases as the vehicle approaches the mid-span. However, the frequency shows the opposite trend when vehicle/bridge frequency ratio is less than 1. The variation of the second order frequency in four cases is insignificant. Therefore, the first order frequency is studied further. Fig. 13(b) illustrates the amplified first order frequencies. When the vehicle/bridge frequency ratio is less than 1, the frequency variation becomes more obvious as the frequency ratio increases. On the other hand, when the frequency ratio exceeds 1, the frequency variation decreases with the increase in the frequency ratio.

To investigate the effect of the vehicle mass on the time-varying characteristics of the bridge, the vehicle stiffness is maintained at a constant value of K_v. As the vehicle mass ranges from 10000 kg to 50000 kg, four different vehicle mass cases, i.e., 10000 kg, 18000 kg, 27000 kg and 45000 kg, are considered. Table 6 lists the mechanical properties of VBI system with four different vehicle masses. The vehicle/bridge frequency ratio decreases as the vehicle mass increases.

The first two frequencies of bridge identified by using AR-EWT+LMSST for different vehicle mass (Case2, Case5, Case6 and Case7) are shown in Fig. 14. The variation of the second order frequency in four cases is insignificant and the first order frequencies in four cases exhibit roughly half sine wave variations. Like vehicle stiffness, the effect of vehicle mass on the frequency of bridge in VBI system is also associated with the vehicle/bridge frequency ratio. However, the influence of vehicle mass on the frequency ratio is opposite to that of stiffness. An increase in vehicle mass will result in

Table 5 Mechanical properties of VBI system for four different vehicle models

Case	Vehicle stiffness	Vehicle mass	Vehicle/bridge frequency ratio(FR)	Vehicle/bridge mass ratio (MR)
1	2 K_v	18000 kg	1.46	0.11
2	K_v	18000 kg	1.03	0.11
3	0.76 K_v	18000 kg	0.9	0.11
4	0.66 K_v	18000 kg	0.84	0.11

Table 6 Mechanical properties of VBI system with four different vehicle masses

Case	Vehicle stiffness	Vehicle mass	Vehicle/bridge frequency ratio(FR)	Vehicle/bridge mass ratio (MR)
2	K_v	18000 kg	1.03	0.11
5	K_v	10000 kg	1.46	0.055
6	K_v	27000 kg	0.84	0.17
7	K_v	45000 kg	0.65	0.28

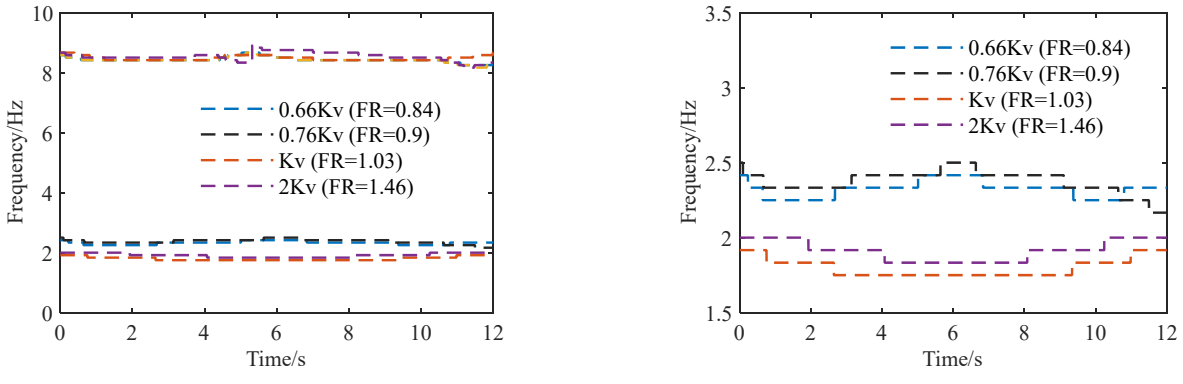

(a) First two order frequencies (b) First order frequencies

Fig. 13 Identified frequencies of bridge for different vehicle stiffness

a decrease in frequency ratio. The first order frequency pattern (Fig. 14(b)) differs when the frequency ratio is greater than 1 or less than 1, and it is similar with the pattern shown in Fig. 13(b).

To investigate the influence of vehicle/bridge mass ratio, the overall stiffness of the vehicle is adjusted while changing the mass of the vehicle to ensure the same frequency ratio. Since the frequency ratio in actual engineering is typically greater than 1, the frequency ratio is controlled at 1.03. The mass ratios of three cases are 0.11, 0.17 and 0.28, respectively. The mechanical properties of VBI system with different vehicle/bridge mass ratios are shown in Table 7.

As shown in Fig. 15, keeping the vehicle/bridge frequency ratio at 1.03 and changing the mass ratio results in a half sine wave change in the first order frequency (Case2, Case8 and Case9). The first order frequency of the bridge decreases as the vehicle approaches the mid-span. With the increase of vehicle/bridge mass ratio, the variation in the first order frequency becomes more significant. Although Case2 and Case8 show no apparent variation in the second order frequency, when the mass ratio reaches 0.28 (Case9), the frequency variation becomes more obvious.

4.2.2 Vehicle speed

The vehicle in Case 1 is driven over the bridge at speed of 7.2 km/h, 10.8 km/h, 14.4 km/h, and 18 km/h, respectively. The road surface remained smooth throughout these simulated cases. The first two order frequencies under different vehicle speeds identified by AR-EWT+LMSST are shown in Fig. 16. The frequency variations are basically the same under different vehicle speeds, indicating that the speed of the vehicle driving over the bridge has no significant impact on the frequency of the bridge. Table 8 presents the RMSE and MAE values of identified IFs of bridge in VBI system under different vehicle speeds. As the vehicle speed increases, the RMSE and MAE values of the first and second order frequencies increase. This means that the identification accuracy decreases as the vehicle speed increases. The reduction of interaction time between the vehicle and bridge as the vehicle speed increases, results in a decrease in the number of acceleration data available for analysis. This adversely affects the accuracy of the AR-

Table 7 Mechanical properties of VBI system with different vehicle/bridge mass ratios

Case	Vehicle stiffness	Vehicle mass	Vehicle/bridge frequency ratio(FR)	Vehicle/bridge mass ratio (MR)
2	K_v	18000 kg	1.03	0.11
8	1.5 K_v	27000 kg	1.03	0.17
9	2.5 K_v	45000 kg	1.03	0.28

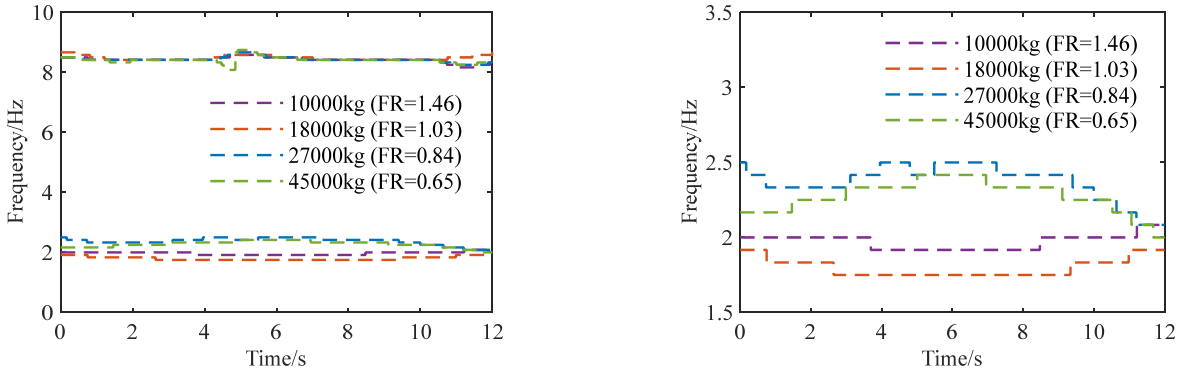

(a) First two order frequencies (b) First order frequencies

Fig. 14 Identified frequencies of bridge for four different Vehicle masses

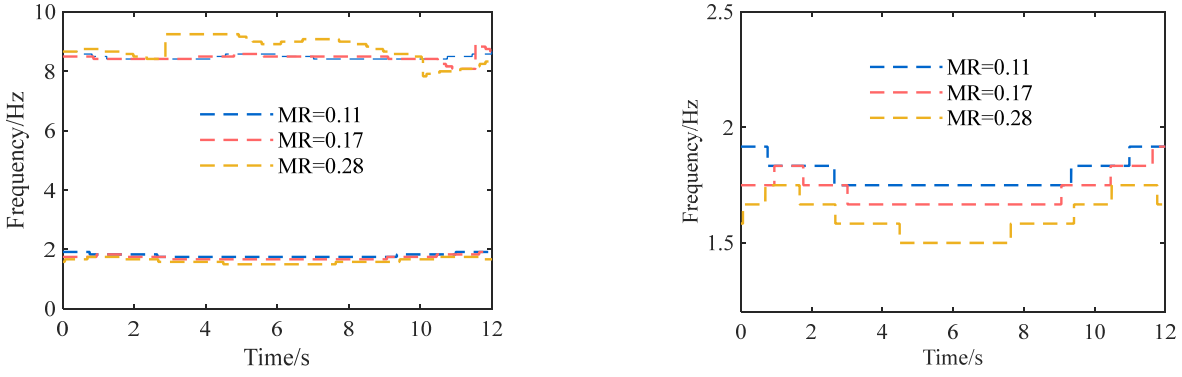

(a) First two order frequencies (b) First order frequencies

Fig. 15 Identified frequencies of bridge for three different vehicle/bridge mass ratios

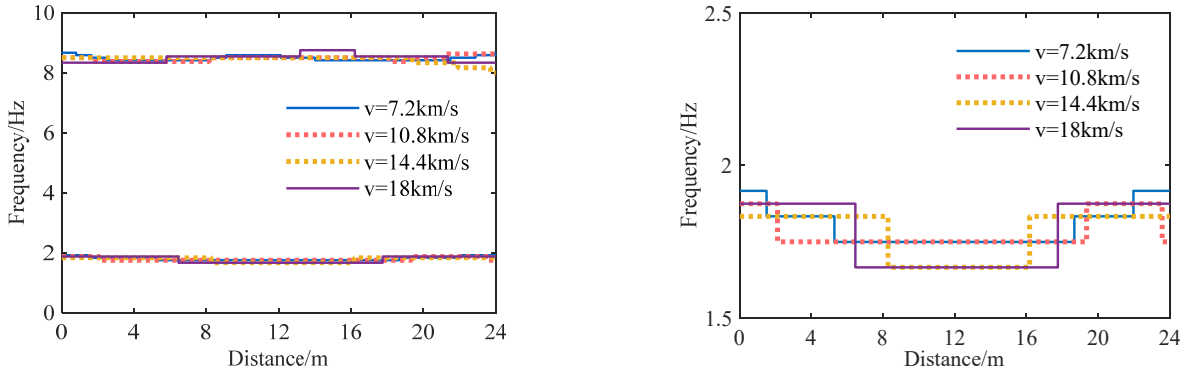

(a) First two order frequencies (b) First order frequencies

Fig. 16 Identified frequencies of bridge for four different vehicle speeds

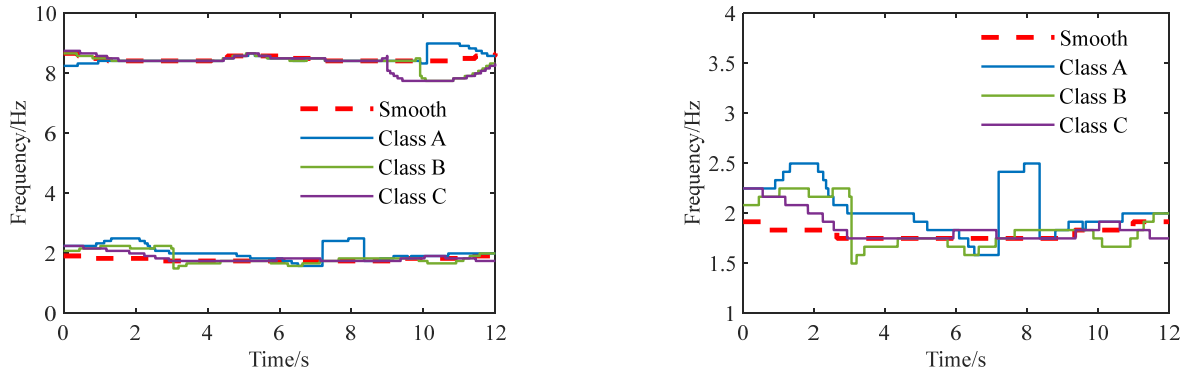

(a) First two order frequencies (b) First order frequencies

Fig. 17 Identified frequencies of bridge for different road surface roughness

Table 8 RMSE and MAE values of identified IFs of bridge in VBI system under different vehicle speeds

Frequency order	Indexes	Vehicle speed			
		7.2 km/h	10.8 km/h	14.4 km/h	18 km/h
1	RMSE	0.0259	0.0516	0.0619	0.0642
	MAE	0.0223	0.0382	0.0560	0.0589
2	RMSE	0.0775	0.0817	0.1067	0.1391
	MAE	0.0575	0.0690	0.0787	0.1231

EWT+LMSST method in identifying frequencies of the bridge.

4.2.3 Road surface roughness

According to the international standard ISO 8608, three classes of road surface roughness, namely A, B, and C, are selected for simulation, and the acceleration response of the bridge at L/4 position is calculated for these classes. The proposed AR-EWT+LMSST method is used to identify the first two frequencies of the bridge under a moving vehicle. As shown in Fig. 17, the first and second order frequencies present evident fluctuations and the first order frequency doesn't exhibit a clear half sine wave trend with the existence of road surface roughness. The impact of road surface roughness on the VBI system is substantially uncertain, resulting in disorderly variations in frequency.

5. Experimental verification

5.1 Experimental setup

A laboratory VBI model is established to verify the feasibility and effectiveness of AR-EWT+LMSST method in identifying the IF of bridge in VBI system. The experimental setup of the VBI model system is shown in Fig. 18. As shown in Fig. 18(a), the bridge model consists of three steel beams. The leading beam and the trailing beam are 2 m in length, and are used for the acceleration and deceleration of the vehicle, respectively. The testing beam is 5 m in length and five accelerometers are installed at intervals of 1/8 L, 1/4 L, 1/2 L, 3/4 L, and 7/8 L from the left end of the test beam. The elastic modulus of the beam is 2.1×10^5 MPa, its cross-sectional area is $3400\ \text{mm}^2$ and

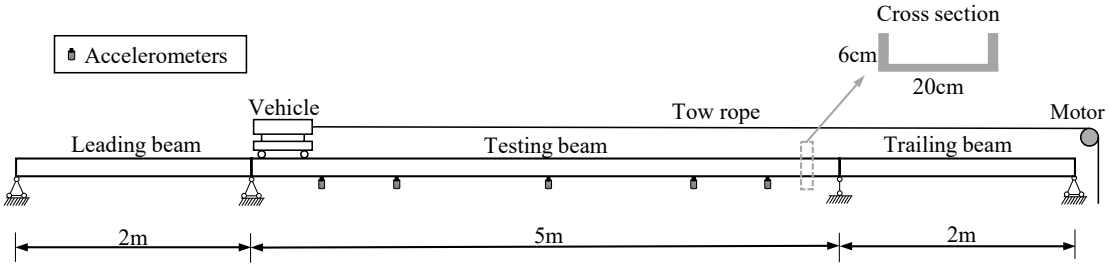

(a) Schematic diagram of the VBI model system

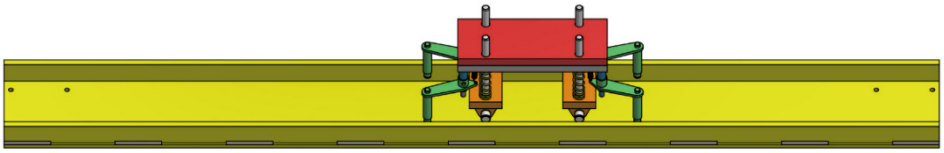

(b) Model of testing beam and vehicle

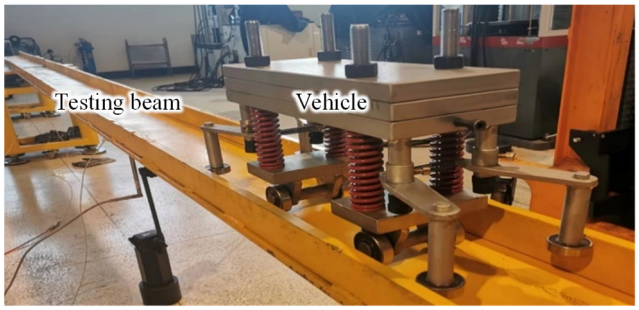

(c) Picture of testing beam and vehicle

Fig. 18 Experimental setup

(a) Accelerometer

(b) The HBM dynamic signal acquisition system

Fig. 19 Data acquisition equipment

Table 9 Mechanical properties of vehicle models

Case	Vehicle speed	Vehicle mass
1	1.0 m/s	26.7 kg
2	1.0 m/s	14.7 kg
3	0.56 m/s	26.7 kg
4	0.56 m/s	14.7 kg

its mass per unit length is 27.1 kg/m. A two-axle vehicle model moves inside the steel channel beams driven by an electrical motor, as displayed in Figs. 18(b) and 18(c). A HBM dynamic signal acquisition system (Fig. 19(a)) and accelerometers (Fig. 19(b)) measured the vertical acceleration responses of the testing beam when the vehicle travels crossing the testing beam. The sampling frequency of recorded acceleration responses is 200 Hz. The measured first two order natural frequencies of the testing beam without the vehicle are 6.67 Hz and 24.85 Hz, respectively.

5.2 Parametric analysis

The AR-EWT+LMSST method is used to identify the bridge frequency from measured bridge vibration acceleration responses in the VBI system. Four cases with different vehicle mass and vehicle speed are considered, and the properties of vehicle models are shown in Table 9.

5.2.1 Vehicle mass

Two vehicle models with different mass are shown in Fig. 20. Fig. 21 shows the vertical acceleration responses of testing beam measured at the L/4 point when the vehicle model crosses the testing beam with speed of 1.0 m/s, i.e., Case 1 and Case 2. Figs. 22 and 23 show the LMSST spectrum identified by using AR-EWT+LMSST for Case 1 and Case 2, respectively. The extracted IFs from the

(a) Vehicle model I (b) Vehicle model II

Fig. 20 Two vehicle models

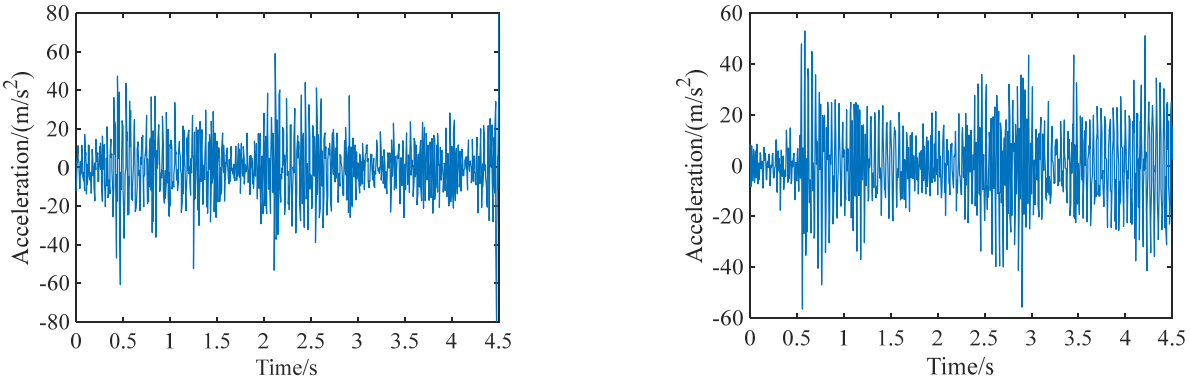

(a) Case 1 (b) Case 2

Fig. 21 Vertical acceleration responses of testing beam measured at the L/4 point

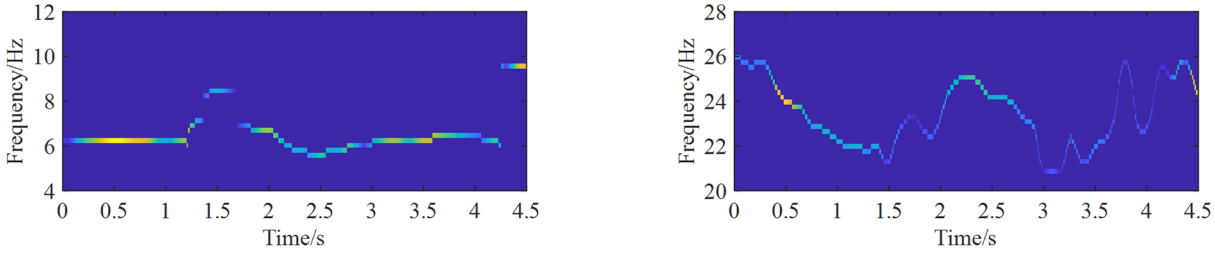

(a) First order frequency (b) Second order frequency

Fig. 22 LMSST spectrum for Case 1

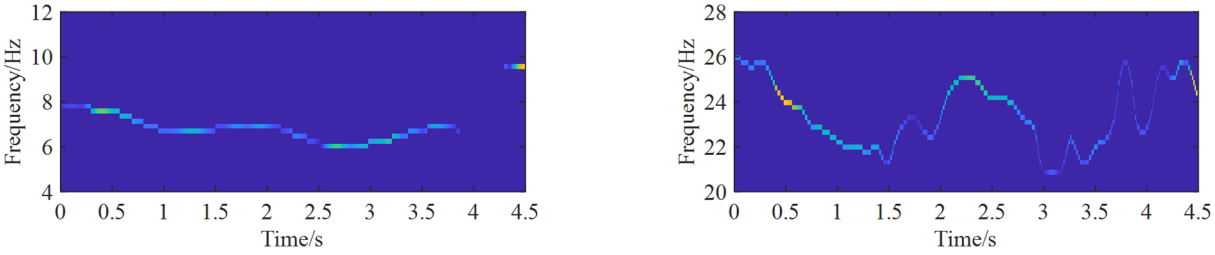

(a) First order frequency (b) Second order frequency

Fig. 23 LMSST spectrum for Case 2

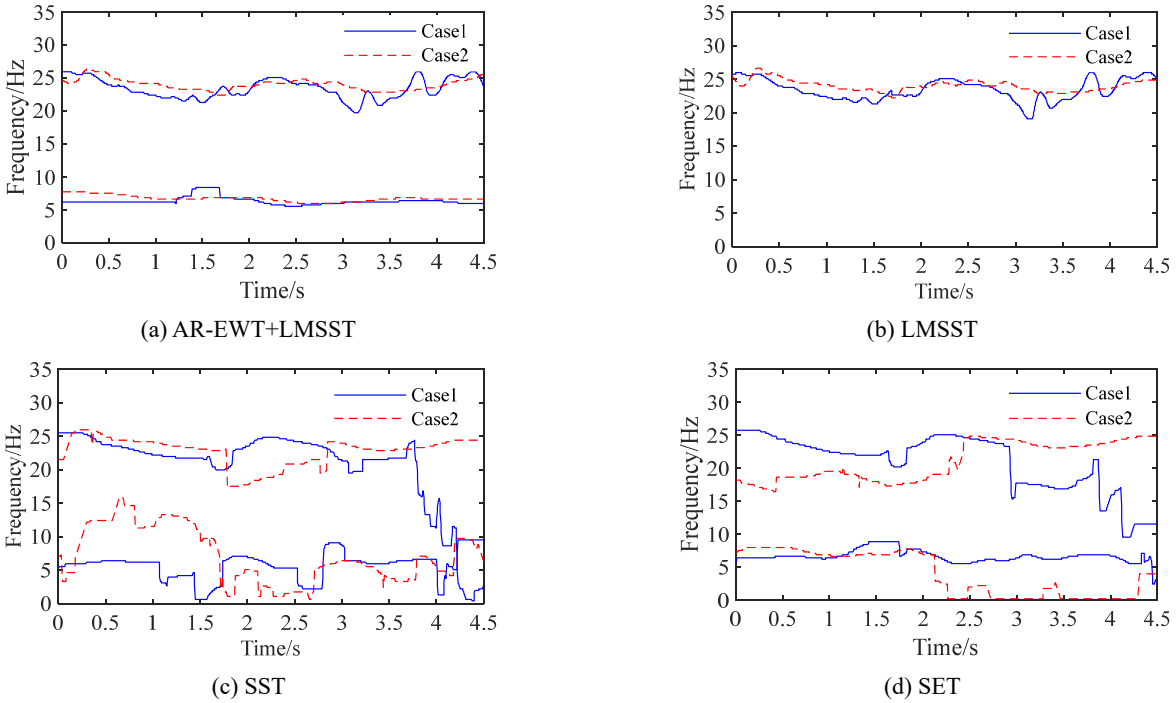

(a) AR-EWT+LMSST (b) LMSST

(c) SST (d) SET

Fig. 24 Identified IFs of the testing beam for Case 1 and Case 2

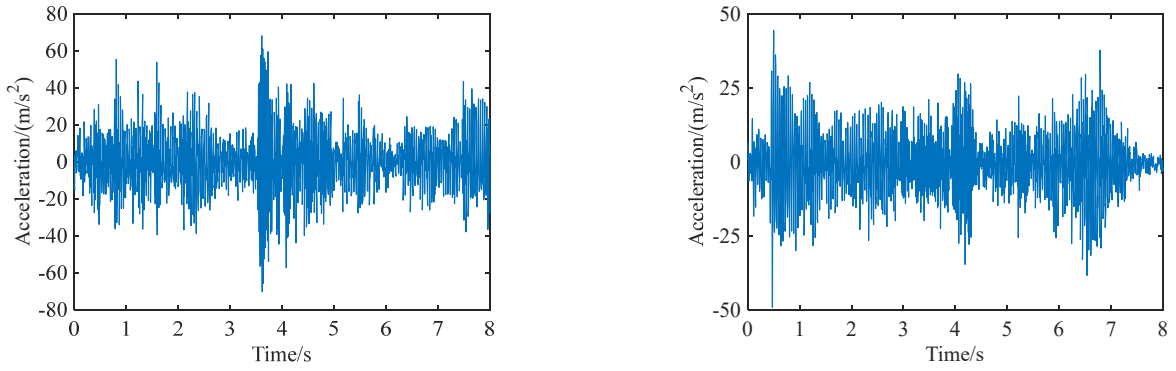

(a) Case 3 (b) Case 4

Fig. 25 Vertical acceleration responses of testing beam measured at the L/4 point

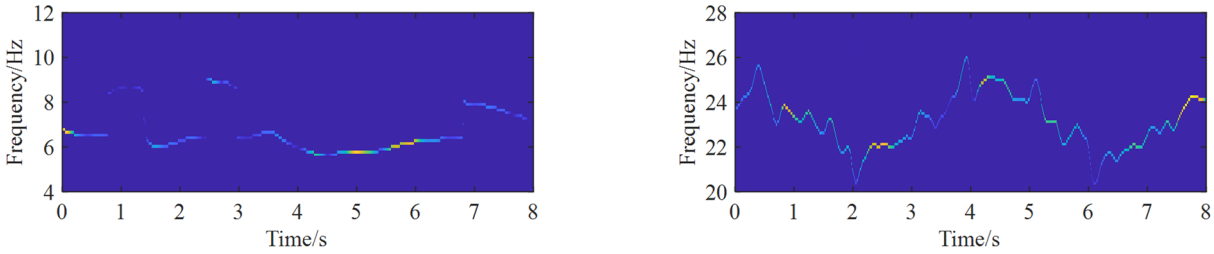

(a) First order frequency (b) Second order frequency

Fig. 26 LMSST spectrum for Case 3

LMSST spectrum (Figs. 22 and 23) are shown in Fig. 24(a). Furthermore, for comparison, the SST, SET, and LMSST methods are also used to analyze the vertical acceleration responses of testing beam, and the identified IFs are shown in Figs. 24(b)-(d). LMSST method fails to identify the first order frequency of the testing beam due to the low energy of the first order frequency, and the frequencies obtained by using SST and SET methods fluctuates greatly. The results demonstrate that the proposed AR-EWT+LMSST method can track the frequency variation of the testing beam

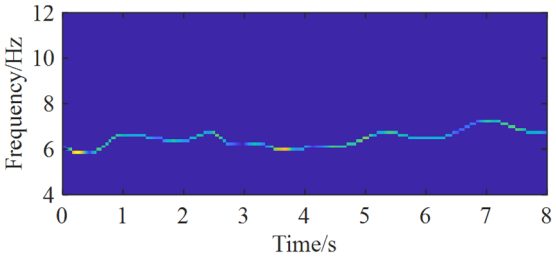

(a) First order frequency

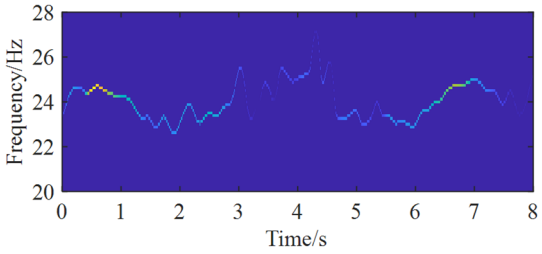

(b) Second order frequency

Fig. 27 LMSST spectrum for Case 4

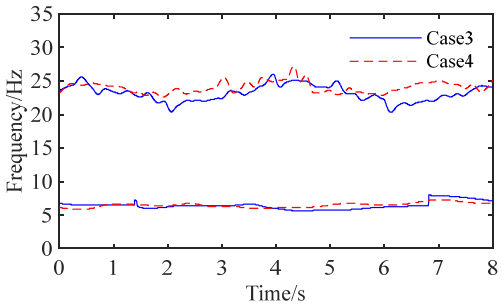

(a) AR-EWT+LMSST

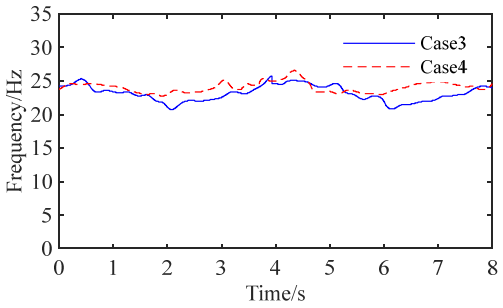

(b) LMSST

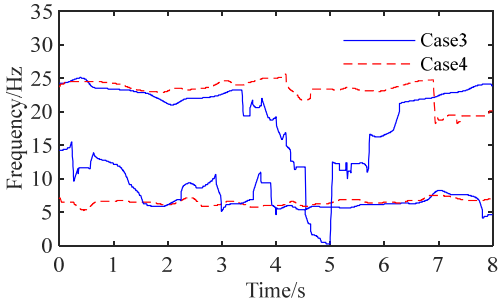

(c) SST

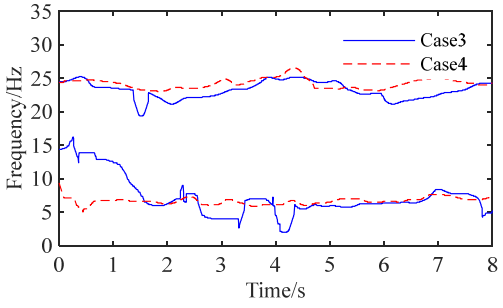

(d) SET

Fig. 28 Identified IFs of the testing beam for Case 3 and Case 4

effectively and accurately. As shown in Fig. 24(a), from the comparison between Case 1 and Case 2, it can be observed that the changing trends of the testing beam frequencies are similar, and larger vehicle mass leads to more drastic frequency variation.

5.2.2 Vehicle speed

Fig. 25 shows the vertical acceleration responses of testing beam measured at the L/4 point when the vehicle model crosses the testing beam with speed of 0.56 m/s, i.e., Case 3 and Case 4. Figs. 26 and 27 show the LMSST spectrum identified by using AR-EWT+LMSST for Case 3 and Case 4, respectively. The identified IFs by using the AR-EWT+LMSST, SST, SET, and LMSST methods are shown in Figs. 28(a)-(d), respectively. As shown in Figs. 28(a)-(d), the identified IFs by using the AR-EWT+LMSST method exhibit the highest level of clarity (Fig. 28(a)). However, LMSST method fails to identify the first order frequency of testing beam due to its low energy (Fig. 28(b)), and the identified IFs by using SST and SET methods show severe fluctuations (Figs. 28(c)-(d)). It can be seen from Fig. 28(a) that the frequency variation of testing beam under the heavy vehicle is higher than the light vehicle. Comparison between Figs. 28(a) and 24(a) shows that the changing trend of IFs obtained under lower vehicle speed is similar to that obtained under higher vehicle speed. Therefore, vehicle speed has no significant effect on the frequency of the bridge in VBI system.

6. Conclusions

An accurate time-frequency analysis method that combines AR-EWT and LMSST is proposed to identify the time-varying IFs of the bridge in the VBI system. AR-EWT is adopted to decompose the vibration responses of the bridge into mono-component signals, and then LMSST is employed to identify the IFs of each mono-component signal. The AR-EWT combined with the LMSST method (AR-EWT+LMSST) can resolve the problem that LMSST cannot effectively identify the multi-component signals with weak amplitude components. Numerical simulations and laboratory model experiment of the VBI system verified that the proposed AR-EWT+LMSST method can

effectively identify the time-varying IFs of the bridge in VBI system. The effect of vehicle characteristics (stiffness and mass), vehicle speed, and road roughness on the frequency variation of bridge in VBI system are further investigated by using the proposed AR-EWT+LMSST method. Compared to the IFs identified by using SST, SET and LMSST method, the proposed AR-EWT+LMSST method has obvious superiority in identifying the IFs of the bridge in the VBI system.

Acknowledgments

The authors are grateful for the financial support from the National Natural Science Foundation of China (Grant Nos. 52078486 and 52278233), the National Key Research and Development Program of China (Grant No. 2021YFE0105600), the Key Project for Scientific and Technological Cooperation Scheme of Jiangxi Province (Grant Nos. 20212BDH80022 and 20223BBH80002).

References

Bettinelli, L., Thannen, B., Stollwitzer, A. and Fink, J. (2022), "Comparison of different approaches for considering vehicle-bridge-interaction in dynamic calculations of high-speed railway bridges", *Eng. Struct.*, **270**, 114897. https://doi.org/10.1016/j.engstruct.2022.114897

Cantero, D., Hester, D. and Brownjohn, J. (2017), "Evolution of bridge frequencies and modes of vibration during truck passage", *Eng. Struct.*, **152**, 452-464. https://doi.org/10.1016/j.engstruct.2017.09.039

Daubechies, I., Liu, J. and Wu, H.T. (2011), "Synchrosqueezed wavelet transforms: An empirical mode decomposition-like tool", *Appl. Comput. Harmon. Anal.*, **30**(2), 243-261. https://doi.org/10.1016/j.acha.2010.08.002

Di Matteo, A., Fiandaca, D. and Pirrotta, A. (2022), "Smartphone-based bridge monitoring through vehicle-bridge interaction: analysis and experimental assessment", *J. Civil Struct. Health Monitor.*, **12**(6), 1329-1342. https://doi.org/10.1007/s13349-022-00593-1

Feldman, M. (2014), "Hilbert transform methods for nonparametric identification of nonlinear time varying vibration systems", *Mech. Syst. Signal Proc.*, **47**(1-2), 66-77. https://doi.org/10.1016/j.ymssp.2012.09.003

Gilles, J. (2013), "Empirical wavelet transform", *IEEE Trans. Signal Process.*, **61**(16), 3999-4010. https://doi.org/10.1109/TSP.2013.2265222

Glatz, B. and Fink, J. (2021), "A redesigned approach to the additional damping method in the dynamic analysis of simply supported railway bridges", *Eng. Struct.*, **241**, 112415. https://doi.org/10.1016/j.engstruct.2021.112415

González, A., Covián, E. and Casero, M. (2023), "Verifying the suitability of uncoupled numerical methods for solving vehicle-bridge interaction problems", *Struct. Infrastruct. Eng.*, **19**(10), 1407-1424. https://doi.org/10.1080/15732479.2022.2033276

Jin, N., Dertimanis, V.K., Chatzi, E.N., Dimitrakopoulos, E.G. and Katafygiotis, L.S. (2022), "Subspace identification of bridge dynamics via traversing vehicle measurements", *J. Sound Vib.*, **523**, 116690. https://doi.org/10.1016/j.jsv.2021.116690

Kalra, M., Kumar, S. and Das, B. (2020), "Seismic signal analysis using empirical wavelet transform for moving ground target detection and classification", *IEEE Sens. J.*, **20**(14), 7886-7895. https://doi.org/10.1109/JSEN.2020.2980857

Kim, C.Y., Jung, D.S., Kim, N.S., Kwon, S.D. and Feng, M.Q. (2003), "Effect of Vehicle mass on natural frequencies of bridges measured from traffic-induced vibration", *Earthq. Eng. Eng. Vib.*, **2**, 109-115. https://doi.org/10.1007/BF02857543

Kong, X., Cai, C.S. and Kong, B. (2016), "Numerically extracting bridge modal properties from dynamic responses of moving vehicles", *J. Eng. Mech.*, **142**(6), 04016025. https://doi.org/10.1061/(ASCE)EM.1943-7889.0001033

Kumar, R., Singh, V. and Ismail, M. (2023), "Post-Earthquake Damage Identification of Buildings with LMSST", *Buildings*, **13**(7), 1614. https://doi.org/10.3390/buildings13071614

Li, J.T., Zhu, X.Q., Law, S.S. and Samali, B. (2020), "Time-varying characteristics of bridges under the passage of vehicles using synchroextracting transform", *Mech. Syst. Signal Proc.*, **140**, 106727. https://doi.org/10.1016/j.ymssp.2020.106727

Li, J.T., Guo, J. and Zhu, X.Q. (2021), "Time-varying parameter identification of bridges subject to moving vehicles using ridge extraction based on empirical wavelet transform", *Int. J. Struct. Stab. Dyn.*, **21**(4), 2150046. https://doi.org/10.1142/S0219455421500462

Li, Y.L., He, W.Y., Ren, W.X., Chen, Z.W. and Li, J.F. (2022), "Modal identification of time-varying vehicle-bridge system using a single sensor", *Smart. Struct. Syst., Int. J.*, **30**(1), 107-119. https://doi.org/10.12989/sss.2022.30.1.107

Liu, J.L., Wang, Z.C., Ren, W.X. and Li, X.X. (2015), "Structural time-varying damage detection using synchrosqueezing wavelet transform", *Smart. Struct. Syst., Int. J.*, **15**(1), 119-133. https://doi.org/10.12989/sss.2015.15.1.119

Luo, Z.J., Liu, T., Yan, S.Z. and Qian, M.B. (2018), "Revised empirical wavelet transform based on auto-regressive power spectrum and its application to the mode decomposition of deployable structure", *J. Sound Vib.*, **431**, 70-87. https://doi.org/10.1016/j.jsv.2018.06.001

Mahdavi, A., Kahoo, A.R., Radad, M. and Monfared, M.S. (2021), "Application of the local maximum synchrosqueezing transform for seismic data", *Digit. Signal Prog.*, **110**, 102934. https://doi.org/10.1016/j.dsp.2020.102934

Matsuoka, K., Kaito, K. and Sogabe, M. (2020), "Bayesian time-frequency analysis of the vehicle-bridge dynamic interaction effect on simple-supported resonant railway bridges", *Mech. Syst. Signal Proc.*, **135**, 106373. https://doi.org/10.1016/j.ymssp.2019.106373

Merainani, B., Rahmoune, C., Benazzouz, D. and Ould Bouamama, B. (2017), "A novel gearbox fault feature extraction and classification using Hilbert empirical wavelet transform, singular value decomposition, and SOM neural network", *J. Vib. Control*, **24**(12), 2512-2531. https://doi.org/10.1177/1077546316688991

Mostafa, N., Di Maio, D., Loendersloot, R. and Tinga, T. (2021), "Extracting the time-dependent resonances of a vehicle-bridge interacting system by wavelet synchrosqueezed transform", *Struct. Control. Health Monitor.*, **28**(12), e2833. https://doi.org/10.1002/stc.2833

Nagarajaiah, S. and Varadarajan, N. (2005), "Short time Fourier transform algorithm for wind response control of buildings with variable stiffness TMD", *Eng. Struct.*, **27**(3), 431-441. https://doi.org/10.1016/j.engstruct.2004.10.015

Oberlin, T., Meignen, S. and Perrier, V. (2015), "Second-order synchrosqueezing transform or invertible reassignment? Towards ideal time-frequency representations", *IEEE Trans. Signal Process.*, **63**(5), 1335-1344. https://doi.org/10.1109/TSP.2015.2391077

Stancioiu, D. and Ouyang, H. (2016), "Optimal vibration control of beams subjected to a mass moving at constant speed", *J. Vib. Control*, **22**(14), 3202-3217. https://doi.org/10.1177/1077546314561814

Stoura, C.D. and Dimitrakopoulos, E.G. (2020), "Additional

damping effect on bridges because of vehicle-bridge interaction", *J. Sound Vib.*, **476**, 115294. https://doi.org/10.1016/j.jsv.2020.115294

Stoura, C.D., Paraskevopoulos, E., Dimitrakopoulos, E.G. and Natsiavas, S. (2021), "A Dynamic Partitioning Method to solve the vehicle-bridge interaction problem", *Comput. Struct.*, **251**, 106547. https://doi.org/10.1016/j.compstruc.2021.106547

Tan, C.J. and Uddin, N. (2020), "Hilbert transform based approach to improve extraction of "drive-by" bridge frequency", *Smart. Struct. Syst., Int. J.*, **25**(3), 265-277. https://doi.org/10.12989/sss.2020.25.3.265

Tan, C.J., Zhao, H., Obrien, E.J., Uddin, N. and Kim, C.W. (2023), "Exploring Time-Varying Characteristics in Drive-By Bridge Frequency Extraction with the Second-Order Synchrosqueezing Transform", *J. Bridge Eng.*, **28**(4), 04023010. https://doi.org/10.1061/JBENF2.BEENG-5979

Thakur, G. and Wu, H.T. (2011), "Synchrosqueezing-based recovery of instantaneous frequency from nonuniform samples", *SIAM J. Math. Anal.*, **43**(5), 2078-2095. https://doi.org/10.1137/100798818

Wan, X., Huang, T.L. and Chen, H.P. (2020), "Improved empirical wavelet transform for modal parameters identification of civil engineering structures under ambient excitations", *J. Vib. Eng*, **33**(2), 219-230. [In Chinese] https://doi.org/10.16385/j.cnki.issn.1004-4523.2020.02.001

Yang, Y. and Nagarajaiah, S. (2014), "Blind identification of damage in time-varying systems using independent component analysis with wavelet transform", *Mech. Syst. Signal Proc.*, **47**(1-2), 3-20. https://doi.org/10.1016/j.ymssp.2012.08.029

Yang, Y.B., Cheng, M.C. and Chang, K.C. (2013), "Frequency variation in vehicle-bridge interaction systems", Int. *J. Struct. Stab. Dyn.*, **13**(2), 1350019. https://doi.org/10.1142/S0219455413500193

Yu, G., Yu, M.J. and Xu, C.Y. (2017), "Synchroextracting Transform", *IEEE Trans. Ind. Electron.*, **64**(10), 8042-8054. https://doi.org/10.1109/TIE.2017.2696503

Yu, G., Wang, Z.H., Zhao, P. and Li, Z. (2019), "Local maximum synchrosqueezing transform: An energy-concentrated time-frequency analysis tool", *Mech. Syst. Signal Proc.*, **117**, 537-552. https://doi.org/10.1016/j.ymssp.2018.08.006

Zhu, X.Q. and Law, S.S. (2003), "Identification of moving interaction forces with incomplete velocity information", *Mech. Syst. Signal Proc.*, **17**(6), 1349-1366. https://doi.org/10.1006/mssp.2002.1577